Distinct roles of cell wall biogenesis in yeast morphogenesis as revealed by multivariate analysis of high-dimensional morphometric data

Hiroki Okada[a], Shinsuke Ohnuki[a], Cesar Roncero[b], James B. Konopka[c], and Yoshikazu Ohya[a]

[a]Department of Integrated Biosciences, Graduate School of Frontier Sciences, University of Tokyo, Kashiwa, Chiba 277-8561, Japan; [b]Instituto de Biología Funcional y Genómica and Departamento de Microbiología y Genética, CSIC/Universidad de Salamanca, 37007 Salamanca, Spain; [c]Department of Molecular Genetics and Microbiology, Stony Brook University, Stony Brook, NY 11794

ABSTRACT The cell wall of budding yeast is a rigid structure composed of multiple components. To thoroughly understand its involvement in morphogenesis, we used the image analysis software CalMorph to quantitatively analyze cell morphology after treatment with drugs that inhibit different processes during cell wall synthesis. Cells treated with cell wall–affecting drugs exhibited broader necks and increased morphological variation. Tunicamycin, which inhibits the initial step of *N*-glycosylation of cell wall mannoproteins, induced morphologies similar to those of strains defective in α-mannosylation. The chitin synthase inhibitor nikkomycin Z induced morphological changes similar to those of mutants defective in chitin transglycosylase, possibly due to the critical role of chitin in anchoring the β-glucan network. To define the mode of action of echinocandin B, a 1,3-β-glucan synthase inhibitor, we compared the morphology it induced with mutants of Fks1 that contains the catalytic domain for 1,3-β-glucan synthesis. Echinocandin B exerted morphological effects similar to those observed in some *fks1* mutants, with defects in cell polarity and reduced glucan synthesis activity, suggesting that echinocandin B affects not only 1,3-β-glucan synthesis, but also another functional domain. Thus our multivariate analyses reveal discrete functions of cell wall components and increase our understanding of the pharmacology of antifungal drugs.

INTRODUCTION

The fungal cell wall is a rigid structure that plays important roles in the establishment and maintenance of cell shape (Klis *et al.*, 2006). Without the cell wall, fungal cells could not form their unique morphology. Cells of the budding yeast *Saccharomyces cerevisiae* have an oval shape, surrounded by the cell wall formed during vegetative cell growth. Dynamic remodeling of the yeast cell wall occurs during the cell cycle and is coordinated during cell morphogenetic events, including bud emergence, apical bud growth, isotropic bud growth, and cell division (Latgé, 2007).

Based on detailed analyses of yeast cell wall composition, it was proposed that it exhibits a highly organized dynamic network structure (Kollár *et al.*, 1997). The cell wall is composed of interconnected filamentous polysaccharides and nonfilamentous glycoproteins. A major filamentous component is 1,3-β-glucan, whose nonreducing ends function as sites for the covalent attachment of other polysaccharides (Klis *et al.*, 2006). 1,6-β-Glucan is another filamentous component, but it is relatively short and a minor component of the cell wall. Highly branched 1,6-β-glucan chains are found at the external face of the 1,3-β-glucan network. Chitin is an additional minor component normally deposited in a ring in the neck between a mother cell and its emerging bud, in the primary septum during division, and in the lateral walls of newly separated daughter cells, where it serves as an anchor for the glucan network (Orlean, 2012). The

major nonfilamentous cell wall components are mannoproteins, which are mannose-containing glycoproteins. These heavily glycosylated proteins are typically found on the exterior of the cell wall. Most mannoproteins are glycosylphosphatidylinositol–anchored proteins and are connected to 1,6-β-glucan chains. Thus, covalent linkages between the various components of the cell wall give rise to its elastic and plastic properties, providing a strong, continuous fabric.

The fact that the different types of yeast cell wall components are interconnected suggests that the disruption of individual cell wall biosynthetic pathways would result in similar morphological phenotypes. Alternatively, the contribution of different components to cell morphology may differ because the physical strength and flexibility of the filamentous and nonfilamentous components vary. Several studies examined the effects of perturbing the synthesis or the cross-linking of cell wall components (de Groot *et al.*, 2001; Nishiyama *et al.*, 2002; Schmidt *et al.*, 2003, 2005; Blanco *et al.*, 2012). However, qualitative observation by eye has limited power to resolve the morphological differences caused by the mutation of genes encoding the enzymes involved in cell wall synthesis. To date, no quantitative morphological analyses of cell wall mutant strains have been performed.

To examine yeast cell morphology quantitatively, we developed an automatic image processing system called CalMorph (Ohtani *et al.*, 2004). This system is a high-throughput, high-resolution image processing software package that enables the quantification of 501 cell morphology parameters from fluorescence images of the cell wall, actin, and nuclear DNA of yeast cells (Ohya *et al.*, 2005). On the basis of a morphological analysis of the 4718 haploid nonessential gene deletion mutants, we created a morphological database named the *Saccharomyces cerevisiae* Morphological Database (SCMD; http://yeast.gi.k.u-tokyo.ac.jp; Saito *et al.*, 2004). Analysis of the data for this large set of mutants revealed significant new relationships between morphological phenotypes and gene functions (Ohya *et al.*, 2005). Further detailed phenotypic analysis of clusters of mutants with similar phenotypes revealed new insights into complex cellular pathways (Ohnuki *et al.*, 2007; Okada *et al.*, 2010; Yoshida *et al.*, 2013). In addition, we were able to predict the intracellular targets of specific drugs by comparing their morphological effects to the database (Ohnuki *et al.*, 2010; Iwaki *et al.*, 2013).

To gain further insight into the involvement of the cell wall in morphogenesis, we quantitatively analyzed the morphological changes induced by echinocandin B (EB), tunicamycin (TM), and nikkomycin Z (NZ), drugs that block cell wall biosynthesis pathways. Specifically, EB is a noncompetitive inhibitor of 1,3-β-glucan synthase (GS; Sawistowska-Schröder *et al.*, 1984; Douglas, 2001), TM targets *N*-acetylglucosamine (GlcNAc) phosphotransferase, which plays a role in the biosynthesis of mannoproteins (Barnes *et al.*, 1984), and NZ is a competitive inhibitor of chitin synthase (Cabib, 1991). Multivariate analyses of the morphological changes induced by these drugs, as well as a comparison of the cell wall mutants, revealed discrete functions of the cell wall components in determining cell morphology.

RESULTS
Morphological effects of cell wall–affecting drugs
The morphological effects of treating haploid yeast with drugs that perturb the cell wall (EB, TM, and NZ) were examined by using fluorescence microscopy to observe the cell wall, actin, and nuclear DNA. Visual inspection revealed that cells treated with 4 μg/ml EB, 100 ng/ml TM, and 400 μM NZ exhibited abnormal morphologies (Figure 1A). To explore the dose-dependent changes, we quantified

501 morphometric parameters using CalMorph (Ohtani *et al.*, 2004) after treatment with various concentrations of the drugs and performed a principal component analysis (PCA). PCA is an exploratory multivariate statistical technique for simplifying complex data sets, and it has been used for analyzing the effects of dose-dependent changes on morphology (Ohnuki *et al.*, 2012). Figure 1B shows that the first principal component (PC1) scores increased in a dose-dependent manner for each of the cell wall–affecting drugs, suggesting that similar morphological changes were progressively more apparent in the data sets. Next we performed a second PCA to identify dose-dependent parameters that are independent of each other (see *Materials and Methods*). Accordingly, we identified seven, eight, and two representative parameters for EB, TM, and NZ, respectively (Supplemental Figures S1 and S2 and Supplemental Tables S1, a–c, and S2, a–c).

Figure 2 illustrates the morphological changes induced by EB, TM, and NZ, in which all representative parameters significantly affected by the drugs are shown ($p < 0.0001$ after Bonferroni correction using the *t* test), as well as the progression of the cell cycle stages, including unbudded cells (G1), budded cells with a single nucleus (S/G2), and budded cells with two nuclei (M). Of note, treatment with all three drugs resulted in an increased neck width (red). Neck width increased at 0.1–0.3 μm with the EB, TM, and NZ treatments (Figures 1A and 3), suggesting that preservation of the neck structure is a major role of the yeast cell wall. In addition to the unique features for each cell wall–affecting drug (black), we identified features common to EB and TM (green), EB and NZ (blue), and TM and NZ (brown). The morphological features induced by TM overlapped with those induced by EB. As reported previously, the proportion of small budded cells increased after EB treatment (Drgonová *et al.*, 1999). Cells were enlarged after TM treatment, as described previously (Arnold and Tanner, 1982). In addition to the known cell morphological changes, we found that actin and the nucleus were also affected. The nuclear size increased after EB and TM treatment, and actin was delocalized in EB- and NZ-treated cells. These quantitative analyses revealed that each cell wall component had different and distinct functions in cell, actin, and nuclear morphology.

Phenotypic variation after treatment with cell wall–affecting drugs
To investigate phenotypic variations, we compared the distribution of variance with and without cell wall drugs. Among the parameters with notable drug effects (Jonckheere–Terpstra test, $p < 0.05$), the variance was greater in EB-, TM-, and NZ-treated cells (Figure 4, A, D, and G). We found that 65% (128/197), 54% (69/127), and 84% (31/37) of the parameters showed a broad distribution after treatment with EB, TM, and NZ, respectively. Mother cell size (parameter C11-1_A) exhibited marked variance among the five replicates after the EB treatment (Figure 4B). Similarly, the long axis in bud (parameter C107_C) and mother cell fitness for ellipse (parameter C13_C) exhibited greater variance after the TM and NZ treatments, respectively (Figure 4, E and H). Phenotypic variation in each trait can be partitioned into the contribution of variations among the cell population and measurement errors. Significantly greater variations among the cell populations were detected after drug treatments (Figure 4, C, F, and I; $p < 0.05$ after Bonferroni correction, Mann–Whitney *U* test), which suggested that phenotypic variation could be explained in part by variation in the cell population.

Effects of EB, TM, and NZ on cell morphology
To compare the effects of the cell wall–affecting drugs, we plotted dose-dependent morphological changes in a two-dimensional (2D)
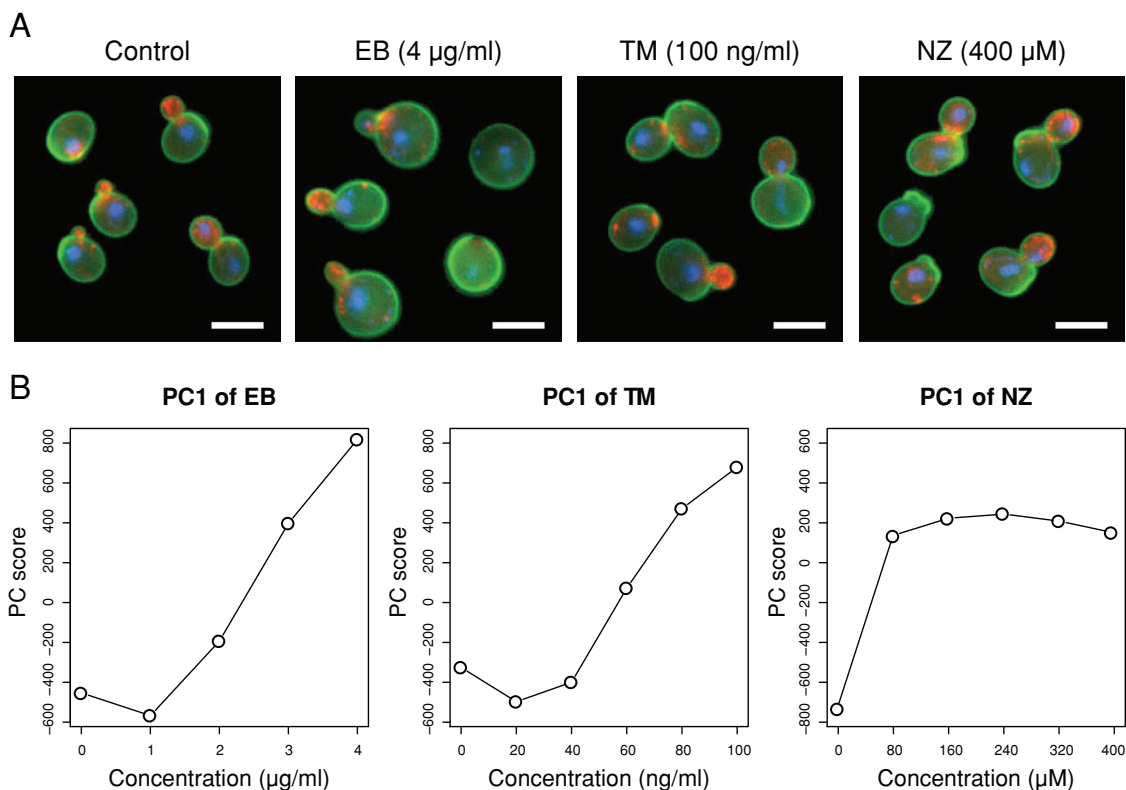
FIGURE 1: Morphological changes induced by cell wall–affecting drugs. (A) Wild-type strains were cultured until the early log phase at 25°C in YPD with EB or TM, and in SD with NZ at the indicated concentrations. Cells were stained with fluorescein isothiocyanate–concanavalin A (green), rhodamine–phalloidin (red), or 4′,6-diamidino-2-phenylindole (blue) to visualize the cell wall, actin, or nucleus, respectively. Bar, 5 µm. (B) Dose-dependent changes in PC1 scores. Morphological data on cells treated with various concentrations of the drugs (n = 5) were subjected to PCA.

space of "similarity" and "dissimilarity." Similar parameters were defined as those with the same direction of changes after treatment with the two drugs, whereas dissimilar parameters exhibited changes in the opposite direction (see *Materials and Methods*). As shown in Figure 5A, similar and dissimilar parameters were located in the first/third quadrants and second/fourth quadrants, respectively. Representative similar and dissimilar features were then extracted by reducing the dimensions by PCA (Figure 5B and Supplemental Figure S3).

The EB and TM treatments are compared in Figure 5C. The EB treatment decreased from the point of origin, but the TM treatment increased with increasing concentrations, separating the effects of the two drugs. Treatment with micafungin, another GS inhibitor, also decreased, similar to EB. Given that micafungin had similar effects to EB, drugs with the same activity showed similar behavior in the similar/dissimilar 2D space.

We also compared EB and NZ treatments and TM and NZ treatments (Supplemental Figure S4). Supplemental Figure S4A shows that EB, NZ, and TM behaved differently but that micafungin acted similarly to EB. TM, NZ, and EB also worked differently in the similar/dissimilar 2D space (Supplemental Figure S4B). Therefore EB, TM, and NZ had distinct effects on cell morphology, as expected from their rather different cellular effects.

Nonessential deletion mutants with morphologies similar to those induced by drug treatments
To validate the analytical system, we compared the morphological profile of cells treated with the cell wall–affecting drugs to those of the nonessential deletion mutants with defects in cell wall–related genes (Lesage and Bussey, 2006; Orlean, 2012). The deletion mutants of the cell wall targets should have similar morphological profiles as cells treated with the cell wall–affecting drugs.

The morphological profiles induced by the TM treatment showed significant similarities to those induced by individual deletions of five genes (*MNN10*, *ANP1*, *OCH1*, *MNN2*, and *HOC1*) that encode mannosyltransferase in the Golgi (Figure 6; p < 0.05 after Bonferroni correction, t test). The correlation coefficient for *mnn10* was 0.59. TM-treated cells were also similar to mutants of *cax4*, a dolichyl pyrophosphate phosphatase that supplies dolichol-linked oligosaccharide substrates for *N*-glycosylation in the endoplasmic reticulum (ER; van Berkel *et al.*, 1999). The Gene Ontology term analysis with the significantly similar 85 gene deletion mutants (p < 0.0001 after Bonferroni correction, t test) showed enrichment of α-1,6-mannosyltransferase activity (Supplemental Table S4). These results are consistent with the mode of action of TM, which blocks *N*-glycosylation (Ballou, 1990; Jigami, 2008).

Of the three chitin synthase mutants, only the *chs1* and *chs3* mutants were viable and therefore testable in our assay. Neither of these mutants was morphologically similar to NZ-treated cells, probably because NZ targets more than one chitin synthase in vivo. NZ-treated cells were morphologically similar to the *utr2* (*crh2*) mutant (Figure 6; r = 0.42), which was defective for the major chitin transglycosylase that functions in the transfer of chitin to 1,3-β- and 1,6-β-glucans (Cabib *et al.*, 2007). In contrast, the morphologies of the *crh1* mutant (defective in minor chitin transglycosylase) and the *crr1* mutant (defective in cross-linking during
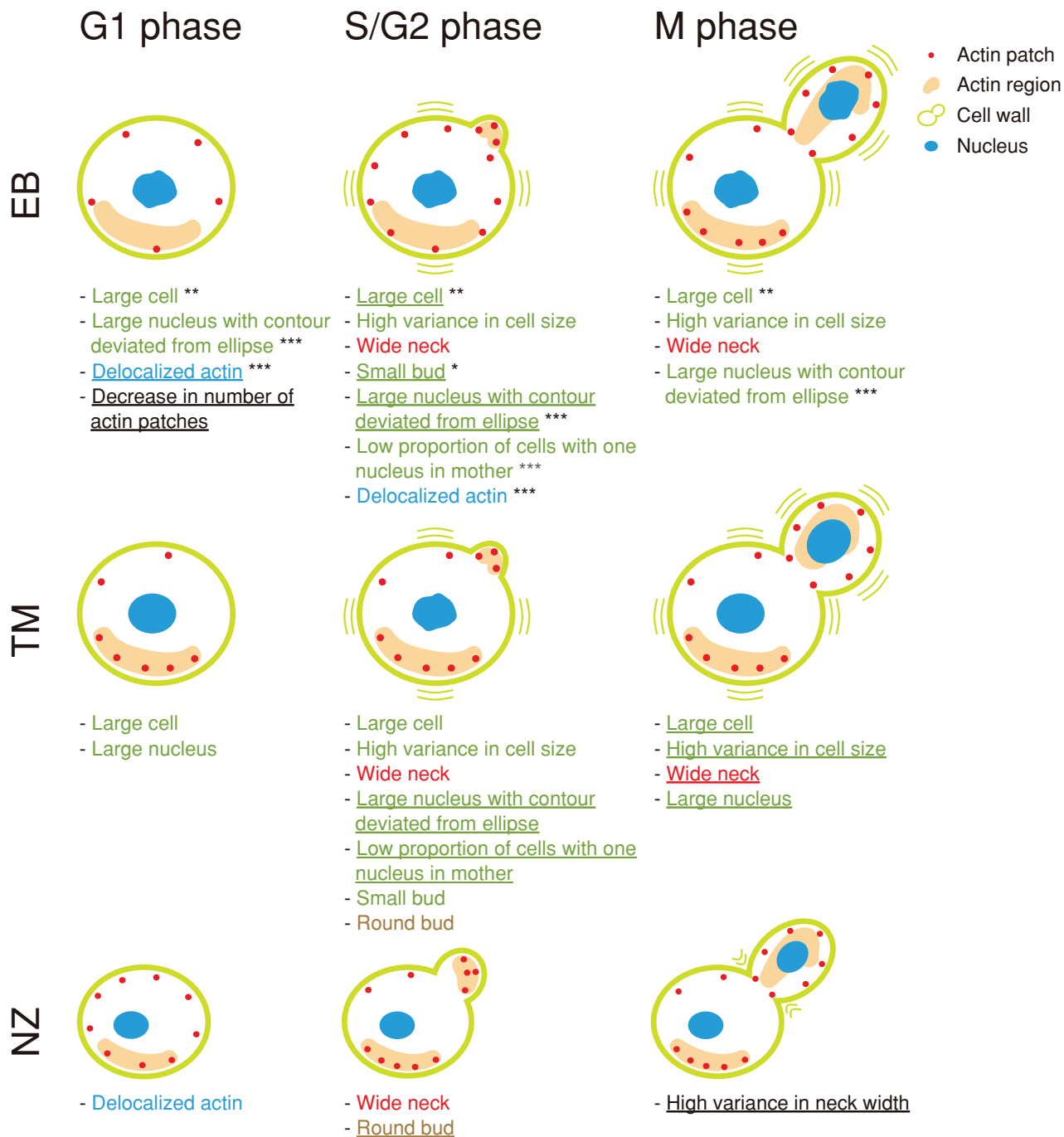
FIGURE 2: Summary of the morphological changes induced by cell wall–affecting drugs. Morphological changes induced by the drugs were analyzed using two-step PCA to identify representative parameters for each drug (see *Materials and Methods*). Representative parameters for each drug (underlined) and those identified for another drug but significantly affected by the indicated drugs are shown with illustrations of the cells (Jonckheere–Terpstra test; <1 false positive was detected by chance at $p = 0.0013$, 0.0052, and 0.0033 for EB, TM, and NZ, respectively; Supplemental Table S3). Colored text indicates shared morphological features among drugs; red, green, blue, and brown represent features shared by EB–TM–NZ, EB–TM, EB–NZ, and TM–NZ , respectively. Asterisks denote features shared by EB and *fks1-ts* mutants; single, double, and triple asterisks indicate features shared by EB and class I and III, class II, and class II and III, respectively (Supplemental Table S5).

sporulation) were different from NZ-treated cells (Rodríguez-Peña *et al.*, 2000; Gómez-Esquer *et al.*, 2004; Cabib *et al.*, 2007). NZ-treated cells were also morphologically similar to mutants lacking *CHS5* (Figure 6), which is involved in the trafficking of Chs3 and Utr2 (Rodríguez-Peña *et al.*, 2002). These results highlight the

critical role that chitin plays in the anchoring of the β-glucan network.

However, EB-treated cells had no resemblance to the deletion mutants of the major (Fks1) and minor (Fks2) subunits of GS (Figure 6). This is consistent with previous observations (Ohnuki *et al.*, 2010;
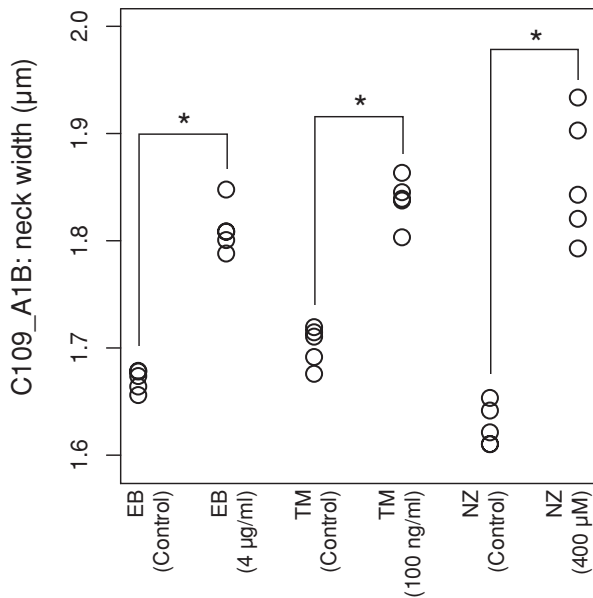
FIGURE 3: Effect of cell wall–affecting drugs on neck width (C109_A1B). Morphological changes induced by treatment with (indicated concentrations) or without (control) the highest drug concentrations are plotted. Asterisk indicates significant difference ($p < 0.05$ by Mann–Whitney U test after Bonferroni correction).

Okada et al., 2010) and is probably due to functional redundancy between Fks1 and Fks2 and/or the multifunctional properties of Fks1 (Ohnuki et al., 2010; Okada et al., 2010). Mutants subsets related to α-1,6-mannosyltransferase were enriched in 84 significantly similar mutants to EB-treated cells ($p < 0.0001$ after Bonferroni correction, t test; Supplemental Table S4), perhaps because EB- and TM-treated cells were somewhat similar.

Morphological similarities with temperature-sensitive *fks1* mutants

Because EB-treated cells were not similar to *fks1Δ* or *fks2Δ* deletion mutants, we compared them with the morphological profiles of temperature-sensitive GS mutants. Because *FKS1* and *FKS2* are redundant genes, we previously created 10 temperature-sensitive *fks1* alleles in an *fks2Δ*-mutant strain background (Figure 7A; Okada et al., 2010). These mutants were classified into three groups (Classes I–III) according to their different phenotypes. After PCA analysis, the morphological profiles of the *fks1* mutants were depicted in a 2D space that described the variety of mutant phenotypes (Figure 7B and Supplemental Figure S5). EB affects GS activity (Sawistowska-Schröder et al., 1984; Douglas, 2001). Because class III mutants showed decreased GS activity, we predicted that EB-treated cells would resemble class III mutants. However, the mapping of PC scores of EB-treated cells indicated similarity to the class II mutants (Figure 7B). Class II mutants showed normal GS activity and exhibited loss of Spa2 localization (Okada et al., 2010). Because Spa2 is a component of the polarisome (Snyder, 1989; van Drogen and Peter, 2002), loss of Spa2 localization is indicative of a cell polarity defect in class II mutants.

To determine whether EB-treated cells had a cell polarity defect, we assessed the localization of Spa2–green fluorescent protein (GFP) in living cells. We confirmed that Spa2 localization was lost in class II but not in class III mutants (Supplemental Figure S6), consistent with previous observations (Okada et al., 2010). We also found that Spa2–GFP localization decreased significantly after EB

treatment (Figure 8), suggesting that EB influenced the regulation of cell polarity by inhibiting Spa2 localization, similar to class II mutants.

We next compared the morphological phenotypes of EB-treated cells with those of the class II and class III mutants. Among the several morphological features of EB-treated cells (Figure 2), either increased cell size or increased ratio of cells with small buds was observed in class II or class III mutants, respectively (Supplemental Table S5). The increased ratio of cells with delocalized actin was common to both classes (Supplemental Table S5). Thus some of the morphological parameters influenced by EB are also affected in class II and III mutants.

EB affects both class II and III domains

Recent topological analysis revealed that EB-resistance mutations accumulated as affected clusters of residues called hot spots at the extracellular surface of Fks1 (Johnson and Edlind, 2012). Hot spots 1–3 are located at amino acid residues of 635–649, 1354–1361, and 690–700, respectively, of Fks1 (Supplemental Table S6). Because these hot spots are considered to be the sites for direct interaction with EB, it is significant that class II and III mutations affected residues near these hot spots in the primary structure of Fks1p (Figure 7A and Supplemental Table S6). To determine whether EB inhibited the function of both class II and class III mutants, we examined the EB sensitivity of each class of GS mutants. Both class II (*fks1-1163*) and class III (*fks1-1154*) mutants failed to grow in the presence of 0.5 μg/ml EB, indicating an EB-sensitive phenotype (Figure 9). In contrast, wild-type and class I mutants (*fks1-1082*) were capable of growth in the presence of 0.5 μg/ml EB. These results suggested that EB affected the functions of the regions of Fks1 that are altered by the class II and class III mutations.

We next determined whether the *fks1* mutants with both class II and III defects were lethal. For this purpose, we constructed strains harboring single-domain (*fks1-1163* and *fks1-1154*) and double-domain (*fks1-11631154*) mutations after a galactose-inducible *FKS1* gene was introduced on a plasmid. We found that the double-domain mutants failed to grow even at 25°C, suggesting that class II and III domains had synergistic effects on the function of Fks1 (Supplemental Figure S7). Thus EB affected two related and important functions of Fks1: 1,3-β-glucan synthesis and cell polarity.

DISCUSSION

We used three drugs (EB, TM, and NZ) that cause distinct types of cell wall damage by inhibiting known targets to characterize the morphological changes induced by inhibiting the biosynthesis of the three major cell wall components, 1,3-β-glucan, mannoproteins, and chitin, in *S. cerevisiae*. Treatment with the three drugs induced several common morphological effects, including increased neck width and morphological variation. However, they also exhibited different effects on cell morphology, indicative of the distinct roles played by the cell wall components in cell morphogenesis. Results of chemical–genetic approaches using TM and NZ were consistent with the classical genetic approach, demonstrating that *N*-linked glycosylation and glucan/chitin cross-linking were important for morphogenesis. Moreover, EB had pleiotropic effects on cell morphology and affected multiple functions of Fks1, including maintenance of cell polarity and 1,3-β-glucan synthesis.

N-glycosylation pathway and cell morphogenesis

Statistical analysis revealed that the TM treatment induced several morphological features. Eight representative parameters were affected in a dose-dependent manner after treatment with TM
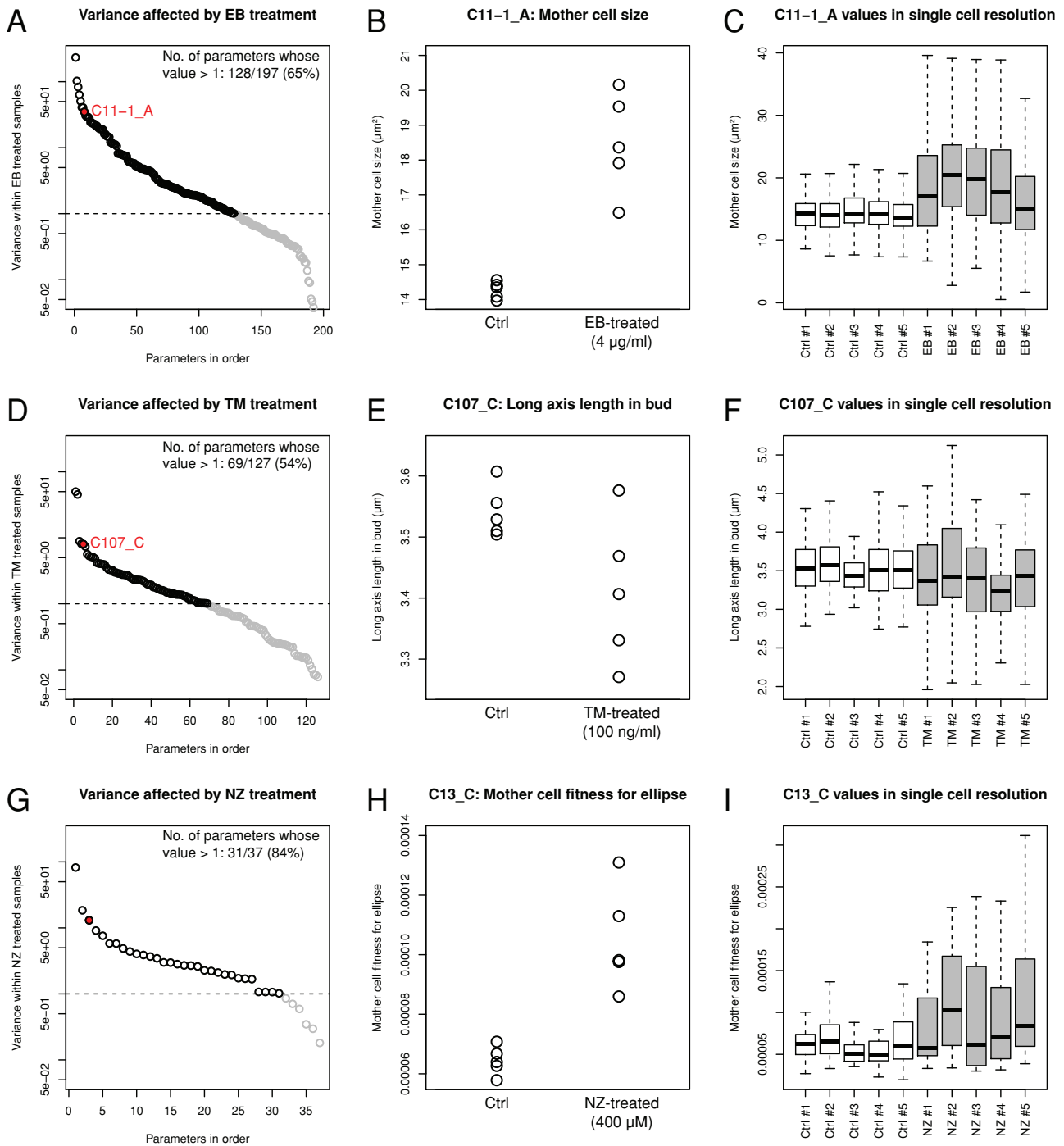
FIGURE 4: Marked morphological variation among drug-treated yeast populations. (A, D, G) Variance in the morphological parameters affected by the drugs (A, EB; D, TM; and G, NZ) was plotted in the highest to lowest order. Black and gray circles indicate parameters of higher and lower variance compared with the control (=1, dashed line), respectively. Red circles denote morphological parameters exemplified in B, E, and H. (B, E, H) Examples of morphological parameters with increased variance upon EB, TM, and NZ treatment. (C, F, I) Distributions of morphological parameters exemplified in B, E, and H visualized using a box plot with single-cell resolution. Gray and white boxes denote single-cell distribution with and without drug treatment, respectively.

(Supplemental Table S2b). For example, mother and daughter cells enlarged, nuclear size increased in unbudded cells, and the neck width increased. The increase in cell size was reported previously (Arnold and Tanner, 1982).

TM blocks the initial step of *N*-glycosylation by inhibiting Alg7 in the ER (Barnes *et al.*, 1984). The morphological profile induced by

the TM treatment showed significant similarity to individual deletions of the genes encoding mannosyltransferase in the Golgi, as well as *cax4*, *die2*, and *ost6*, which mediate *N*-glycosylation in the ER. TM-treated cells were similar to an *och1* mutant (a mutant of *cis*-Golgi α-1,6-mannosyltransferase), deletion mutants of Golgi α-1,6-mannosyltransferase and the M-pol II complex (*mnn10*,
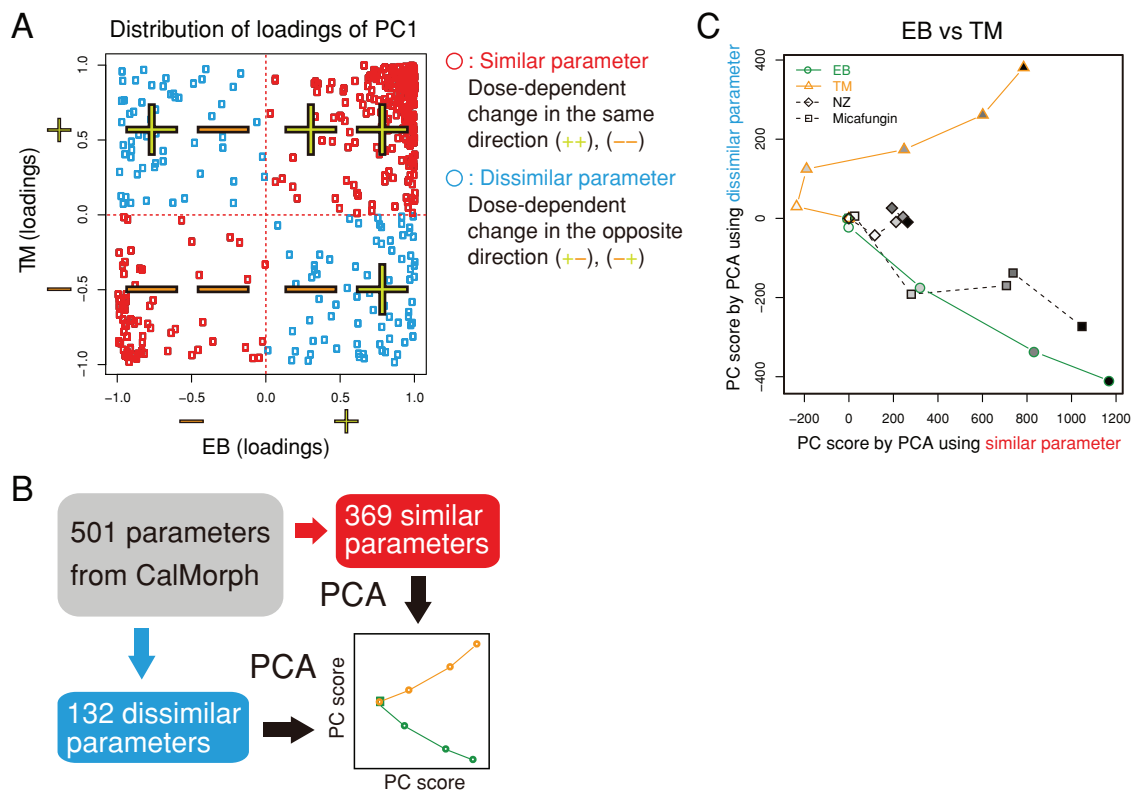
FIGURE 5: Similarity and dissimilarity of the effects of the drugs on cell morphology. (A) Distribution of loadings for PC1 after PCA of the EB and TM data. Of the 501 parameters, 369 were defined as similar (red symbols) due to their distribution in the first/third quadrants; otherwise, 132 were dissimilar parameters that were distributed in the second/fourth quadrants (blue symbols). (B) Schematic representation of the extraction of similar/dissimilar effects on drug treatment. Morphological parameters were assigned to similar or dissimilar parameters based on the loading sign and independently subjected to the second PCA. Dose-dependent effects of the drugs were then visualized in a similar/dissimilar 2D space. (C) Similar and dissimilar effects of EB and TM on cell morphology. Morphological changes induced by NZ and micafungin were mapped onto the 2D space. The grayscale indicates the doses of drugs used (from dilute to concentrated).

anp1, and *hoc1*), and a *mnn2* mutant (a mutant of α-1,2-mannosyltransferase), which are defective in the first, third, and fourth steps, respectively, of outer-chain elongation of *N*-linked oligosaccharides in the Golgi (Jigami, 2008). Mnn9 is also a component of M-pol II (A complex), but forms another mannosyltransferase complex known as M-pol I (V complex), which functions in the second step with Van1 (Hashimoto and Yoda, 1997; Jungmann and Munro, 1998; Jungmann *et al.*, 1999). Given that the morphological phenotypes of *mnn9* and *van1* differ from that of TM-treated cells, M-pol I may play additional roles in cell morphogenesis.

Loss of mannosyltransferase activity reduces protein mannosylation (Lagunas *et al.*, 1986). Mutants defective in early glycosylation reactions exhibit aberrant cell wall assembly (Orłowski *et al.*, 2007). These results suggest that *N*-glycosylation is necessary for the activity or stability of the proteins responsible for cell wall assembly. Unexpectedly, we found that the effects of TM treatment were similar to the effects caused by the single-gene deletion of Ccw12 (Figure 6; *r* = 0.66), highlighting the role of this mannoprotein in cell wall function (Mrsa *et al.*, 1999; Ragni *et al.*, 2011).

Chitin synthesis and cell morphogenesis

NZ had no severe effects on *S. cerevisiae* growth, and therefore its effect on cell morphology was expectedly minor. We found that neck width and bud roundness increased, whereas the ratio of unbudded cells with localized actin decreased. The wide-neck phenotype was reported previously (Schmidt *et al.*, 2003). Note that no changes in nuclear morphology were detected.

Chitin is a polymer of 1,4-β-linked GlcNAc, contributing only 1–2% of the dry weight of the cell wall (Lesage and Bussey, 2006), which serves as a scaffold for anchoring 1,3-β- and 1,6-β-glucans. Chitin occurs in three different and polydispersed forms in the wall. In addition to free chitin, some is bound to 1,3-β-glucan and is present predominantly in the neck region, whereas a lesser amount is found in lateral walls bound to 1,6-β-glucan (Cabib and Durán, 2005; Cabib, 2009). We found that NZ-treated cells were morphologically similar to *utr2*, which was defective in glucan/chitin crosslinking (Cabib *et al.*, 2007; Cabib, 2009). In addition, *chs5* and *pfa4* mutants, but not *chs3*, *chs6*, or *chs7*, all of which contain reduced levels of chitin, also showed a significant correlation with the NZ treatment cells. Of interest, only *chs5* and *pfa4* have additional defects on the intracellular traffic of other proteins, including the mislocalization of Utr2 in the *chs5* mutant (Rodríguez-Peña *et al.*, 2002). These results highlight the critical role of the chitin–glucan linkage in morphogenesis, in clear agreement with a recent proposal (Cabib and Arroyo, 2013), but also uncover a redundant role of the different chitin synthases in forming the chitin–glucan network.

EB affects multiple functions of Fks1

Echinocandin-family drugs (e.g., EB and micafungin) noncompetitively inhibit incorporation of UDP-glucose into 1,3-β-glucan
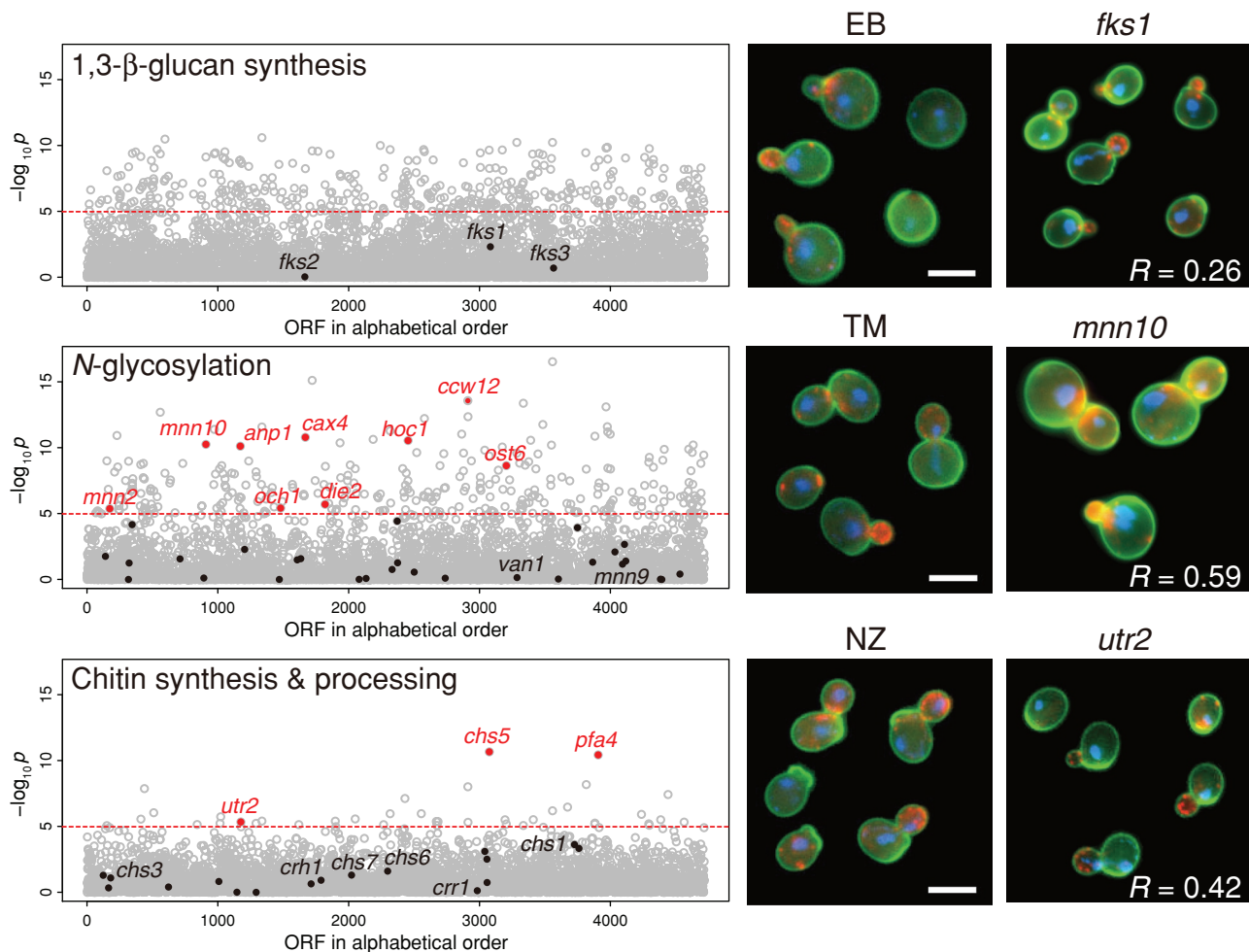
FIGURE 6: Morphological profiling of the cell wall–affecting drugs. The drug-induced morphological profiles were compared with 4718 mutants of nonessential genes, as described previously (Ohnuki *et al.*, 2010). The vertical axis indicates the similarity to each gene deletion mutant as a $-\log_{10} p$ value of a correlation coefficient (*t* test). The horizontal dashed line shows the threshold of $p = 1.06 \times 10^{-5}$ corresponding to a one-sided $p = 0.05$ after Bonferroni correction. Red dots denote cell wall–associated mutants (Lesage and Bussey, 2006; Orlean, 2012), with morphological profiles similar to those of drug-treated cells. Right, representative photographs of wild-type cells after drug treatment and representative deletion mutants (*fks1*, *mnn10*, and *utr2*). *R* is the correlation coefficient between drug-treated and mutant cells. Bar, 5 μm.
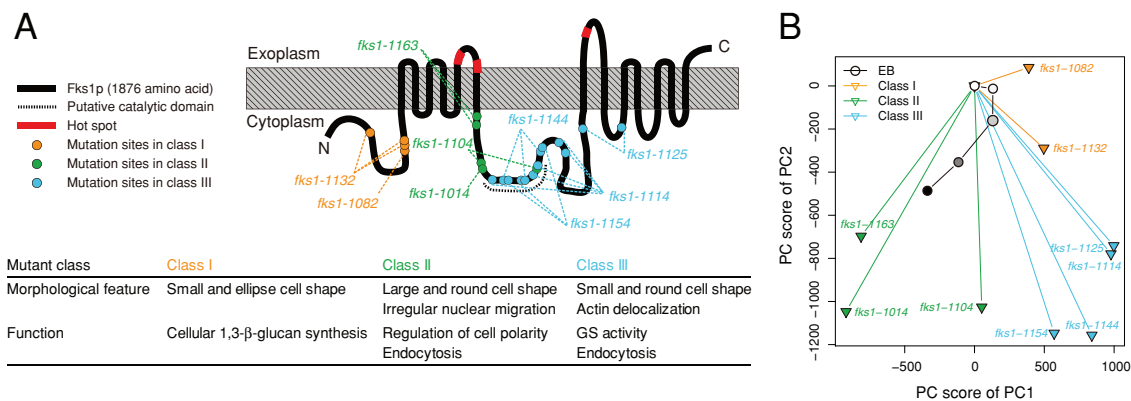

FIGURE 7: Morphological phenotypes of EB-treated and *fks1* cells. (A) Functional map of Fks1p (modified from Okada *et al.*, 2010). The gray-hatched box denotes the plasma membrane. Red symbols on the black line indicate hot spots (the echinocandin resistance–conferring mutations). The amino acids mutated and the hot spots are listed in Supplemental Table S6. (B) PCA of the data sets of EB-treated and *fks1* cells. Morphological data on EB-treated cells were mapped onto the 2D space obtained by PCA of the *fks1-ts* mutant (Okada *et al.*, 2010). The grayscale within the circular symbols indicates the dose of EB used (from dilute to concentrated). PC1 and PC2 explained ~60% of the variance.
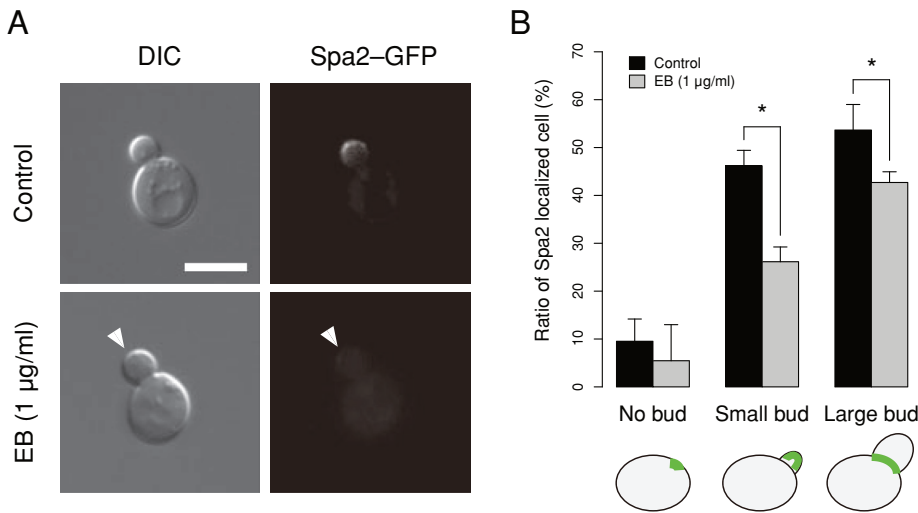
FIGURE 8: Effect of EB on Spa2–GFP localization. (A) YOC5002 (*spa2* [Spa2–GFP]) cells were incubated at 25°C in SD–U medium with EB (1 µg/ml) or DMSO (control solvent) until the early log phase. Cells were then harvested and observed without fixation. The arrowhead indicates the absence of Spa2–GFP localization in the bud. Bar, 5 µm. (B) Spa2–GFP localized cells were enumerated in three independent experiments. The mean of the triplicates is plotted. Error bars denote 1 standard deviation. Asterisk indicates significant difference ($p < 0.05$ by t test after Bonferroni correction).

(Douglas, 2001). This has not been demonstrated directly, but several lines of evidence suggest that Fks1 is a direct target of echinocandins. For example, Fks1 is a putative catalytic subunit of GS (Inoue *et al.*, 1995; Drgonová *et al.*, 1996; Qadota *et al.*, 1996); hot spots—regions of the mutations conferring strong echinocandin resistance—exist exclusively in Fks1 (Douglas, 2001; Perlin, 2007; Johnson *et al.*, 2011); and specific mutations within these hot spots result in differential echinocandin resistance (Johnson *et al.*, 2011; Healey *et al.*, 2012).

Here we demonstrated that EB more strongly affected class II and III *fks1* mutants, which carry substitutions in the cytosolic region. Johnson and Edlind (2012) reported that the three hot spots for echinocandin-resistance mutations affect residues that are located externally and proposed that all hot spot residues are juxtaposed in the three-dimensional structure of Fks1 to form a single echinocandin-binding pocket. Of interest, the residues affected by the class II and III mutations are adjacent to the hot spots, which suggests that binding of EB affects the central cytosolic domains of Fks1.

Preservation of the neck structure of the cell wall

We demonstrated that yeast cells had a broadened neck width after treatment with all cell wall–affecting drugs, suggesting that maintaining a narrow neck is a common function performed by cell wall components. Phenotypic analysis of several cell wall mutants supported this hypothesis. Mutation of genes involved in the outer-chain elongation of *N*-linked oligosaccharides in the Golgi (*OCH1*, *MNN10*, *ANP1*, and *MNN2*), *CAX4* (*N*-glycosylation in the ER), and *CCW12* (mannoprotein) resulted in significantly wider necks (data available at SCMD). Chs5, which is involved in the export of chitin synthase (Santos and Snyder, 1997; Santos *et al.*, 1997), Kre6, which is required for 1,6-β-glucan biosynthesis (Roemer and Bussey, 1991), and 1,3-β-glucanosyltransferase (Gas1), which is required for cell wall assembly; Ram *et al.*, 1998; Popolo and Vai, 1999), were also all necessary to maintain a narrow neck (data available at SCMD). Thus classical genetic and chemical–genetic approaches both resulted in common morphological phenotypes induced by the lesion of cell wall components.

All components of the yeast cell wall are localized at or near the bud neck. The filamentous components 1,3-β-glucan and 1,6-β-glucan are found on the interior of the cell wall around a constriction between the mother and daughter cells. Nonfilamentous component mannoproteins are also localized to this region on the exterior surface. In contrast, chitin is localized at the bud/birth scar and the primary septum. Several explanations of the wide-neck phenotypes caused by cell wall–affecting drugs are possible. Physical strength is presumably required to maintain the curvature structure of the neck. If the network structure of the cell wall is weakened, it may lead to morphological changes of the neck. Alternatively, neck morphology may be determined by many genes, among which those encoding enzymes responsible for synthesis of cell wall components may play important roles. Further studies are required to clarify the molecular mechanism underlying neck morphogenesis and demonstrate how it is related to cell wall functions.
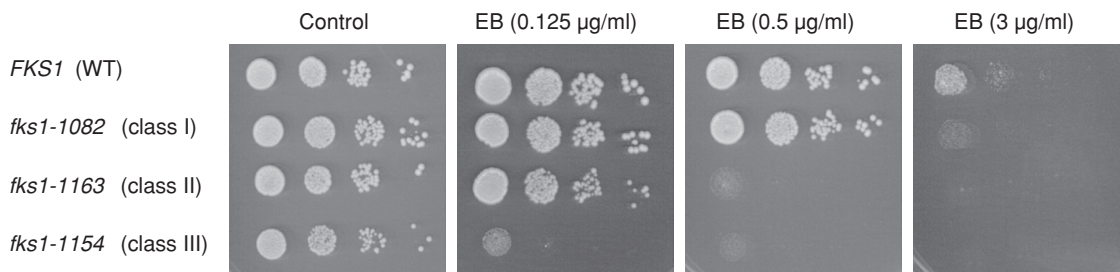

FIGURE 9: EB sensitivity of the *fks1-ts* mutants. Cells were cultured in YPD medium until the log phase and diluted serially to 1×10^6, 1×10^5, 1×10^4, and 1×10^3 cells/ml. Suspensions of 5 µl were dropped on the plates contained EB or DMSO as a control solvent. Plates were incubated at 25°C for 3 d. The experiments were replicated at least twice, and representative results are shown. *FKS1*, *fks1-1082*, *fks1-1154*, and *fks1-1163* indicate YOC4318, YOC4320, YOC4327, and YOC4328, respectively.

Contribution of the cell wall to phenotypic robustness

We demonstrated that yeast cells were highly morphologically variable after perturbation of the cell wall components. We found significantly greater variations between the cell populations after treatment with cell wall–affecting drugs. Levy and Siegal (2008) identified yeast deletion mutants with highly variable phenotypes. In their study, the *anp1* mutant exhibited the second-highest variability in overall morphology and *mnn10* the 14th highest among all nonessential deletion mutants. Mutants (*och1*, *hoc1*, *mnn2*, *cax4*, and *ccw12*) defective in the mannoproteins, *gas1*, and *kre6* were also identified to be highly variable. Although the molecular mechanism is unclear, the cell wall structure likely provides robustness to the cell by protecting the intracellular functional network from environmental conditions.

Multivariate analysis to explore complex phenotypes

We used several multivariate approaches to investigate the complex phenotypes induced by cell wall–affecting drugs. To identify the morphological features after obtaining high-dimensional morphology data, we performed two-step PCA (Ohnuki *et al.*, 2012). This approach allowed us to demonstrate that all cell wall components had roles in the preservation of the neck structure and phenotypic robustness. To predict the gene deletion mutant whose morphological profile would be similar to that of the drug-treated cells, we used a high-content, image-based profiling method (Ohnuki *et al.*, 2010), which validated our analysis and indicated a similar function of chitin synthesis for chitin transglycosylase in morphogenesis. A combination of genetic and statistical analyses facilitated examination of the complex effects of cell wall–affecting drugs. Using these approaches, we determined the mode of action of EB using temperature-sensitive *fks1* mutants, which showed specific loss of the individual functions of Fks1.

Cell wall biosynthesis is a tightly coordinated dynamic biological process. Our results suggest mechanistic roles of the cell wall components in cell morphogenesis and increase our understanding of novel functions of the cell wall and the pharmacology of antifungal drugs. A similar approach could be used to investigate the functions of other cellular components in cell morphology.

MATERIALS AND METHODS

Strains and plasmids

The yeast strains and plasmids used in this study are listed in Supplemental Tables S7 and S8 and are deposited with the National BioResource Project Japan, Yeast Genetic Resource Center (Osaka, Japan). The *fks1* mutants were constructed as described previously (Okada *et al.*, 2010). Y02458 (as BY4741 *his3::KanMX*) was used as the wild-type strain. Standard procedures were used for all DNA manipulations and *Escherichia coli* transformations (Sambrook *et al.*, 1989).

Media and reagents

Yeast-rich medium (YPD) contained 1% Bacto yeast extract (BD Biosciences, San Jose, CA), 2% Bacto peptone (BD Biosciences), and 2% glucose. Yeast synthetic medium (SD or SGS) contained 0.66% Bacto yeast nitrogen base lacking amino acids (BD Biosciences), 2% glucose (SD) or 2% galactose, plus 0.2% sucrose (SGS), and was supplemented with the appropriate nutrients. Luria–Bertani medium for *E. coli* contained 1% Bacto tryptone (BD Biosciences), 0.5% Bacto yeast extract, and 1% NaCl. Stock solutions of 2 mg/ml EB (a gift from O. Kondo, Chugai Pharmaceutical, Tokyo, Japan) or 10 mg/ml TM (Sigma-Aldrich, St. Louis, MO) were prepared in dimethyl sulfoxide (DMSO; Wako Pure Chemical Industries, Osaka, Japan). Stocks

of 10 mM NZ (Sigma-Aldrich) and 10 mg/ml micafungin (Astellas Pharma, Tokyo, Japan) were prepared in distilled water.

Quantification of the effects of drug treatment on cell morphology

Wild-type yeast strains were cultured at 25°C in YPD until the early log phase (~16 h) with 0, 1, 2, 3, or 4 µg/ml EB; 0, 20, 40, 60, 80, or 100 ng/ml TM; or 0, 10, 15, 20, 25, or 30 ng/ml micafungin. Strains treated with NZ (0, 80, 160, 240, 320, or 400 µM) were cultured in SD. The concentrations of cell wall–affecting drugs were determined based on the growth inhibition rates (~10%, excluding NZ, which did not significantly inhibit the growth of *S. cerevisiae*). Cell fixation, staining, and observation were performed as described previously (Ohnuki *et al.*, 2012). Images were analyzed using the image processing software CalMorph (version 1.2), which extracted a total of 501 morphological quantitative values from at least 200 individual cells in each experiment. Images were processed using Photoshop CS2 (Adobe Systems, San Jose, CA) for illustrative purposes.

Statistical analysis

Morphological profiling of the drugs using the Jonckheere–Terpstra test was performed to assess the morphological similarity between the cells treated with the cell wall–affecting drugs and nonessential deletion mutants (Jonckheere, 1954; Ohnuki *et al.*, 2010). Other statistical analyses, including PCA, were performed using R, version 2.14.0 (www.r-project.org/).

Two-step PCA

Before applying PCA to morphological parameters, we transformed five replicated parameters to rank-sum values to unify the distribution of each parameter, as described previously (Ohnuki *et al.*, 2012). PCA was performed using the prcomp of the R function without scaling.

To identify independent morphological features induced by the drugs, we performed a two-step PCA, as described previously (Ohnuki *et al.*, 2012). In the first PCA, morphological data on cells treated with the drugs were subjected to PCA (Supplemental Figure S1). The dose-dependent parameters were correlated with the first principal component (PC1) significantly (Supplemental Table S1, a–c) and had high absolute loading values to PC1. Of the 501 parameters, significant PC loadings in PC1 were observed for 265, 168, and eight parameters in the EB, TM, and NZ data sets, respectively (false discovery rate = 0.1 by *t* test). In the second PCA, data obtained from 122 replicated experiments of wild-type cells (null-distributed data) in the correlated parameters were subjected to PCA after Box–Cox power transformation. The parameter-correlating PCs in the second PCA, explaining 60% of the variance, had significant loadings (>0.5) at *p* < 0.0001 based on the *t* test after Bonferroni correction (Supplemental Figure S2, A and B). Several independent PCs, named in alphabetical order (e.g., PC1, PC2, and PC3 were named PC1a, PC1b, and PC1c, respectively), were extracted for each drug (Supplemental Table S2, a–c). One or two dose-dependent parameters of the various morphological criteria were selected as representative parameters after taking the absolute loading values to each PC (>0.5) and the meaning of the parameters (colored in yellow in Supplemental Table S2, a–c) into account.

Estimation of the variation in cell morphology

Parameters showing notable dose-dependent drug effects were detected using the Jonckheere–Terpstra test (*p* < 0.05). Of the detected parameters (354 parameters in EB, 241 in TM, and 87 in NZ), the "mean" parameters (197, 127, and 37 parameters, respectively)

representing the population average were analyzed further. The data on cells treated with a high concentration of drugs (4 µg/ml EB, 100 ng/ml TM, and 400 µM NZ; $n = 5$) were centered by subtracting the mean and scaled by dividing by the standard deviation of the control cells without drug treatment ($n = 5$) and then used to assess the effects of the drugs on cell morphology.

Extraction of similar/dissimilar effects of drug treatments

After PCA on the morphological data for the drug-treated cells, the loadings of 501 traits for PC1 were plotted on the 2D space of two or three arbitrary drugs. Because PC1 scores of all three drugs increased in a dose-dependent manner, we assumed that the traits correlating with PC1 in the same direction (a positive or negative correlation) between the drugs reflected similar effects. Conversely, traits in different directions reflected dissimilar effects. For pairwise comparisons among the three drugs (EB–TM, EB–NZ, and TM–NZ), we defined similar parameters (369, 289, and 293 traits) and dissimilar parameters (132, 212, and 208 traits, respectively) from 501 traits based on the loadings. To identify the primary effects of the drugs on each set of similar/dissimilar parameters, we applied PCA independently (Supplemental Figure S3) and visualized the distribution of PC1 scores.

Spa2 localization

To assess Spa2 localization, we constructed a plasmid expressing a Spa2–GFP fusion protein with GFP conjugated immediately before the stop codon. A DNA fragment of the *SPA2* open reading frame, with its 0.5-kb-upstream region, was amplified from the *S. cerevisiae* genome by PCR using primers that generated a *Sma*I restriction site at each end. The PCR product was cloned into a low-copy plasmid harboring the *URA3* marker and *GFP*-coding sequence with an *FKS1* terminator to make pYO2642. pYO2642 was then used to transform Y01509, YOC1001, YOC1087, and YOC1089 on SD-without-uracil (SD–U) plates to obtain YOC5002 and YOC5041–5043, respectively. YOC5002 was cultured at 25°C in liquid SD–U with EB (1 µg/ml) or DMSO (control solvent) until the early log phase and harvested. YOC5041–5043 were cultured with SD–U at 25°C until early log phase, followed by additional incubation at 37°C for 2 h. After a brief sonication of cells, Spa2–GFP localization was observed using fluorescence microscopy.

REFERENCES

Arnold E, Tanner W (1982). An obligatory role of protein glycosylation in the life cycle of yeast cells. FEBS Lett 148, 49–53.

Ballou CE (1990). Isolation, characterization, and properties of *Saccharomyces cerevisiae mnn* mutants with nonconditional protein glycosylation defects. Methods Enzymol 185, 440–470.

Barnes G, Hansen WJ, Holcomb CL, Rine J (1984). Asparagine-linked glycosylation in *Saccharomyces cerevisiae*: genetic analysis of an early step. Mol Cell Biol 4, 2381–2388.

Blanco N, Reidy M, Arroyo J, Cabib E (2012). Crosslinks in the cell wall of budding yeast control morphogenesis at the mother-bud neck. J Cell Sci 125, 5781–5789.

Cabib E (1991). Differential inhibition of chitin synthetases 1 and 2 from *Saccharomyces cerevisiae* by polyoxin D and nikkomycins. Antimicrob Agents Chemother 35, 170–173.

Cabib E (2009). Two novel techniques for determination of polysaccharide cross-links show that Crh1p and Crh2p attach chitin to both beta(1-6)- and beta(1-3)glucan in the *Saccharomyces cerevisiae* cell wall. Eukaryot Cell 8, 1626–1636.

Cabib E, Arroyo J (2013). How carbohydrates sculpt cells: chemical control of morphogenesis in the yeast cell wall. Nat Rev Microbiol 11, 648–655.

Cabib E, Blanco N, Grau C, Rodríguez-Peña JM, Arroyo J (2007). Crh1p and Crh2p are required for the cross-linking of chitin to beta(1-6)glucan in the *Saccharomyces cerevisiae* cell wall. Mol Microbiol 63, 921–935.

Cabib E, Durán A (2005). Synthase III-dependent chitin is bound to different acceptors depending on location on the cell wall of budding yeast. J Biol Chem 280, 9170–9179.

de Groot PW *et al.* (2001). A genomic approach for the identification and classification of genes involved in cell wall formation and its regulation in *Saccharomyces cerevisiae*. Comp Funct Genomics 2, 124–142.

Douglas CM (2001). Fungal beta(1,3)-D-glucan synthesis. Med Mycol 39, Suppl 1)55–66.

Drgonová J, Drgon T, Roh DH, Cabib E (1999). The GTP-binding protein Rho1p is required for cell cycle progression and polarization of the yeast cell. J Cell Biol 146, 373–387.

Drgonová J, Drgon T, Tanaka K, Kollár R, Chen GC, Ford RA, Chan CS, Takai Y, Cabib E (1996). Rho1p, a yeast protein at the interface between cell polarization and morphogenesis. Science 272, 277–279.

Gómez-Esquer F, Rodríguez-Peña JM, Díaz G, Rodriguez E, Briza P, Nombela C, Arroyo J (2004). *CRR1*, a gene encoding a putative transglycosidase, is required for proper spore wall assembly in *Saccharomyces cerevisiae*. Microbiology 150, 3269–3280.

Hashimoto H, Yoda K (1997). Novel membrane protein complexes for protein glycosylation in the yeast Golgi apparatus. Biochem Biophys Res Commun 241, 682–686.

Healey KR, Katiyar SK, Raj S, Edlind TD (2012). CRS-MIS in *Candida glabrata*: sphingolipids modulate echinocandin-Fks interaction. Mol Microbiol 86, 303–313.

Inoue SB, Takewaki N, Takasuka T, Mio T, Adachi M, Fujii Y, Miyamoto C, Arisawa M, Furuichi Y, Watanabe T (1995). Characterization and gene cloning of 1,3-beta-D-glucan synthase from *Saccharomyces cerevisiae*. Eur J Biochem 231, 845–854.

Iwaki A, Ohnuki S, Suga Y, Izawa S, Ohya Y (2013). Vanillin inhibits translation and induces messenger ribonucleoprotein (mRNP) granule formation in *Saccharomyces cerevisiae*: application and validation of high-content, image-based profiling. PLoS One 8, e61748.

Jigami Y (2008). Yeast glycobiology and its application. Biosci Biotechnol Biochem 72, 637–648.

Johnson ME, Edlind TD (2012). Topological and mutational analysis of *Saccharomyces cerevisiae* Fks1. Eukaryot Cell 11, 952–960.

Johnson ME, Katiyar SK, Edlind TD (2011). New Fks hot spot for acquired echinocandin resistance in *Saccharomyces cerevisiae* and its contribution to intrinsic resistance of *Scedosporium* species. Antimicrob Agents Chemother 55, 3774–3781.

Jonckheere AR (1954). A test of significance for the relation between M rankings and K ranked categories. Br J Stat Psychol 7, 93–100.

Jungmann J, Munro S (1998). Multi-protein complexes in the cis Golgi of *Saccharomyces cerevisiae* with alpha-1,6-mannosyltransferase activity. EMBO J 17, 423–434.

Jungmann J, Rayner JC, Munro S (1999). The *Saccharomyces cerevisiae* protein Mnn10p/Bed1p is a subunit of a Golgi mannosyltransferase complex. J Biol Chem 274, 6579–6585.

Klis FM, Boorsma A, De Groot PWJ (2006). Cell wall construction in *Saccharomyces cerevisiae*. Yeast 23, 185–202.

Kollár R, Reinhold BB, Petráková E, Yeh HJ, Ashwell G, Drgonová J, Kapteyn JC, Klis FM, Cabib E (1997). Architecture of the yeast cell wall. Beta(1→6)-glucan interconnects mannoprotein, beta(1→3)glucan, and chitin. J Biol Chem 272, 17762–17775.

Lagunas R, DeJuan C, Benito B (1986). Inhibition of biosynthesis of *Saccharomyces cerevisiae* sugar transport system by tunicamycin. J Bacteriol 168, 1484–1486.

Latgé J-P (2007). The cell wall: a carbohydrate armour for the fungal cell. Mol Microbiol 66, 279–290.

Lesage G, Bussey H (2006). Cell wall assembly in *Saccharomyces cerevisiae*. Microbiol Mol Biol Rev 70, 317–343.

Levy SF, Siegal ML (2008). Network hubs buffer environmental variation in *Saccharomyces cerevisiae*. PLoS Biol 6, e264.

Mrsa V, Ecker M, Strahl-Bolsinger S, Nimtz M, Lehle L, Tanner W (1999). Deletion of new covalently linked cell wall glycoproteins alters the electrophoretic mobility of phosphorylated wall components of *Saccharomyces cerevisiae*. J Bacteriol 181, 3076–3086.

Nishiyama Y, Uchida K, Yamaguchi H (2002). Morphological changes of *Candida albicans* induced by micafungin (FK463), a water-soluble echinocandin-like lipopeptide. J Electron Microsc (Tokyo) 51, 247–255.

Ohnuki S, Kobayashi T, Ogawa H, Kozone I, Ueda J-Y, Takagi M, Shin-Ya K, Hirata D, Nogami S, Ohya Y (2012). Analysis of the biological activity of a novel 24-membered macrolide JBIR-19 in *Saccharomyces cerevisiae* by the morphological imaging program CalMorph. FEMS Yeast Res 12, 293–304.

Ohnuki S, Nogami S, Kanai H, Hirata D, Nakatani Y, Morishita S, Ohya Y (2007). Diversity of Ca²⁺-induced morphology revealed by morphological phenotyping of Ca²⁺-sensitive mutants of *Saccharomyces cerevisiae*. Eukaryot Cell 6, 817–830.

Ohnuki S, Oka S, Nogami S, Ohya Y (2010). High-content, image-based screening for drug targets in yeast. PLoS One 5, e10177.

Ohtani M, Saka A, Sano F, Ohya Y, Morishita S (2004). Development of image processing program for yeast cell morphology. J Bioinform Comput Biol 1, 695–709.

Ohya Y *et al.* (2005). High-dimensional and large-scale phenotyping of yeast mutants. Proc Natl Acad Sci USA 102, 19015–19020.

Okada H, Abe M, Asakawa-Minemura M, Hirata A, Qadota H, Morishita K, Ohnuki S, Nogami S, Ohya Y (2010). Multiple functional domains of the yeast l,3-β-glucan synthase subunit Fks1p revealed by quantitative phenotypic analysis of temperature-sensitive mutants. Genetics 184, 1013–1024.

Orlean P (2012). Architecture and biosynthesis of the *Saccharomyces cerevisiae* cell wall. Genetics 192, 775–818.

Orłowski J, Machula K, Janik A, Zdebska E, Palamarczyk G (2007). Dissecting the role of dolichol in cell wall assembly in the yeast mutants impaired in early glycosylation reactions. Yeast 24, 239–252.

Perlin DS (2007). Resistance to echinocandin-class antifungal drugs. Drug Resist Updat 10, 121–130.

Popolo L, Vai M (1999). The Gas1 glycoprotein, a putative wall polymer cross-linker. Biochim Biophys Acta 1426, 385–400.

Qadota H, Python CP, Inoue SB, Arisawa M, Anraku Y, Zheng Y, Watanabe T, Levin DE, Ohya Y (1996). Identification of yeast Rho1p GTPase as a regulatory subunit of 1,3-beta-glucan synthase. Science 272, 279–281.

Ragni E, Piberger H, Neupert C, García-Cantalejo J, Popolo L, Arroyo J, Aebi M, Strahl S (2011). The genetic interaction network of *CCW12*, a *Saccharomyces cerevisiae* gene required for cell wall integrity during budding and formation of mating projections. BMC Genomics 12, 107.

Ram AF, Kapteyn JC, Montijn RC, Caro LH, Douwes JE, Baginsky W, Mazur P, van den Ende H, Klis FM (1998). Loss of the plasma membrane-bound protein Gas1p in *Saccharomyces cerevisiae* results in the release of beta1,3-glucan into the medium and induces a compensation mechanism to ensure cell wall integrity. J Bacteriol 180, 1418–1424.

Rodríguez-Peña JM, Cid VJ, Arroyo J, Nombela C (2000). A novel family of cell wall-related proteins regulated differently during the yeast life cycle. Mol Cell Biol 20, 3245–3255.

Rodríguez-Peña JM, Rodriguez C, Alvarez A, Nombela C, Arroyo J (2002). Mechanisms for targeting of the *Saccharomyces cerevisiae* GPI-anchored cell wall protein Crh2p to polarised growth sites. J Cell Sci 115, 2549–2558.

Roemer T, Bussey H (1991). Yeast beta-glucan synthesis: *KRE6* encodes a predicted type II membrane protein required for glucan synthesis *in vivo* and for glucan synthase activity *in vitro*. Proc Natl Acad Sci USA 88, 11295–11299.

Saito TL, Ohtani M, Sawai H, Sano F, Saka A, Watanabe D, Yukawa M, Ohya Y, Morishita S (2004). SCMD: *Saccharomyces cerevisiae* Morphological Database. Nucleic Acids Res 32, D319–22.

Sambrook J, Fritsch EF, Maniatis T (1989). Molecular Cloning: A Laboratory Manual, Cold Spring Harbor, NY: Cold Spring Harbor Laboratory Press.

Santos B, Duran A, Valdivieso MH (1997). *CHS5*, a gene involved in chitin synthesis and mating in *Saccharomyces cerevisiae*. Mol Cell Biol 17, 2485–2496.

Santos B, Snyder M (1997). Targeting of chitin synthase 3 to polarized growth sites in yeast requires Chs5p and Myo2p. J Cell Biol 136, 95–110.

Sawistowska-Schröder ET, Kerridge D, Perry H (1984). Echinocandin inhibition of 1,3-β-D-glucan synthase from *Candida albicans*. FEBS Lett 173, 134–138.

Schmidt M, Strenk ME, Boyer MP, Fritsch BJ (2005). Importance of cell wall mannoproteins for septum formation in *Saccharomyces cerevisiae*. Yeast 22, 715–723.

Schmidt M, Varma A, Drgon T, Bowers B, Cabib E (2003). Septins, under Cla4p regulation, and the chitin ring are required for neck integrity in budding yeast. Mol Biol Cell 14, 2128–2141.

Snyder M (1989). The *SPA2* protein of yeast localizes to sites of cell growth. J Cell Biol 108, 1419–1429.

van Berkel MA, Rieger M, te Heesen S, Ram AF, van den Ende H, Aebi M, Klis FM (1999). The *Saccharomyces cerevisiae CWH8* gene is required for full levels of dolichol-linked oligosaccharides in the endoplasmic reticulum and for efficient N-glycosylation. Glycobiology 9, 243–253.

van Drogen F, Peter M (2002). Spa2p functions as a scaffold-like protein to recruit the Mpk1p MAP kinase module to sites of polarized growth. Curr Biol 12, 1698–1703.

Yoshida M, Ohnuki S, Yashiroda Y, Ohya Y (2013). Profilin is required for Ca²⁺ homeostasis and Ca²⁺-modulated bud formation in yeast. Mol Genet Genomics 288, 317–328.